Stability of XeK_4 compound under extreme conditions

Caiwen Lu, Kang Yang, Wenwen Cui, Jian Hao, Jingming Shi,* and Yinwei Li†
Laboratory of Quantum Functional Materials Design and Application, School of Physics and Electronic Engineering, Jiangsu Normal University, Xuzhou 221116, China

(Received 24 April 2024; revised 10 July 2024; accepted 12 July 2024; published 24 July 2024)

Noble gas elements exhibit chemical reactivity under high pressure, forming novel compounds through reactions with other substances, which has become a recent focus in condensed matter physics research. By combining first-principles calculations with crystal structure prediction methods, we propose six unconventional Xe-K compounds under high pressure, namely Xe_4K, Xe_3K, Xe_3K_2, Xe_2K, XeK, and XeK_4. In addition to previously proposed Xe-rich compounds, we introduce an unconventional K-rich compound, XeK_4, which remains stable over a considerable pressure range from 49 to 104 GPa and a high-pressure phase of Xe_3K. Both XeK_4 and Xe_3K demonstrate metallic properties with a strong ionic Xe-K bond within their stable pressure range. Further *ab initio* molecular dynamics simulations indicate that XeK_4 undergoes a solid-to-liquid transition with increasing temperature, while the other Xe-K compounds maintain solid-state characteristics. The solid or liquid stability pressure ranges of Xe-K compounds cover the pressure and temperature conditions of the Earth's mantle, suggesting that XeK_4 and other Xe-K compounds might act as possible constitutes and exist in the Earth's mantle. These results could provide essential information for understanding the Xe-K compounds and the Xe chemistry at high pressure.

DOI: 10.1103/PhysRevB.110.024111

I. INTRODUCTION

The investigation of materials under extreme conditions has emerged as a prominent frontier in contemporary research, offering profound insights into the fundamental properties and behaviors of substances [1,2]. Among these, noble gases, traditionally known for their inert nature under standard conditions, have garnered increasing attention due to their intriguing reactivity and novel compound formations under high-pressure environments [3–7]. Particularly, xenon (Xe), with its unique electron configuration and versatile bonding capabilities, has become a focal point in the exploration of high-pressure chemistry [3,8–11]. In recent years, advancements in experimental techniques and computational methodologies have enabled researchers to delve into the realm of Xe-containing compounds under extreme pressures [12–16]. This burgeoning field not only sheds light on the fundamental principles governing chemical bonding and phase transitions but also holds significant implications for diverse areas including materials science, geophysics, and planetary science.

Research has found that under extreme high-temperature and high-pressure conditions, Xe can exhibit chemical reactivity and form unconventional compounds that do not exist at ambient conditions through reactions with various substances. As early as 1962, scientists synthesized the first Xe-containing compound, $XePtF_6$, in the laboratory [17], followed by a series of Xe compounds proposed either experimentally or theoretically. The formation mechanisms of these Xe-containing compounds involve a broad range of substances that react with Xe, which can be categorized into several aspects. First, Xe can form van der Waals compounds with inert elements or quasi-inert molecules under high pressure, such as Xe-Ar [15,16] and Xe-NH_3 [3]. On the other hand, Xe can react with certain molecules to form compounds, such as $Xe(O_2)_2$ [18,19], Xe_2O_5 and Xe_3O_2 [20], $Xe_4O_{12}H_{12}$ [9], $4Xe \cdot 24H_2O$ [21], Xe-O [22,23], and $Xe(H_2)_7$ [24]. Additionally, recent studies have shown that Xe can react with minerals within the Earth's interior, leading to the formation of novel Xe-containing minerals under extreme conditions within the Earth, such as XeFe/Ni [25], Xe-Na [26,27], Xe_2FeO_2 [8], Xe-Mg [11], and $XeSiO_2$ [28]. These discovered Xe-containing minerals provide important theoretical explanations for the missing Xe paradox and expand the chemistry of noble gas compounds. Hofman *et al.* estimated that the continental crust contains about 37% of the total K present in the silicate Earth [29]. Subsequently, Fe-K compounds were studied to explain the potassium-containing Earth's core [30]. A recent theoretical study proposes that Xe and K can form compounds under high-pressure conditions [13]. But these compounds are predominantly Xe-rich compounds. Considering the abundant presence of K in the Earth's interior, it remains a crucial research question to investigate whether Xe and K can form K-rich compounds under extreme conditions within the Earth's interior.

In this paper, combining structure predictions and first-principles calculations, we predict the formation of a K-rich compound, XeK_4, and another high-pressure phase of $C2/m$-Xe_3K. The predicted $C2/c$-XeK_4 is stable in a large pressure range from 49 to 104 GPa. Both of $C2/m$-Xe_3K and $C2/c$-XeK_4 exhibit metallic properties with strong ionic K-Xe bonds. Further *ab initio* molecular dynamics (AIMD)

*Contact author: jingmingshi@jsnu.edu.cn
†Contact author: yinwei_li@jsnu.edu.cn

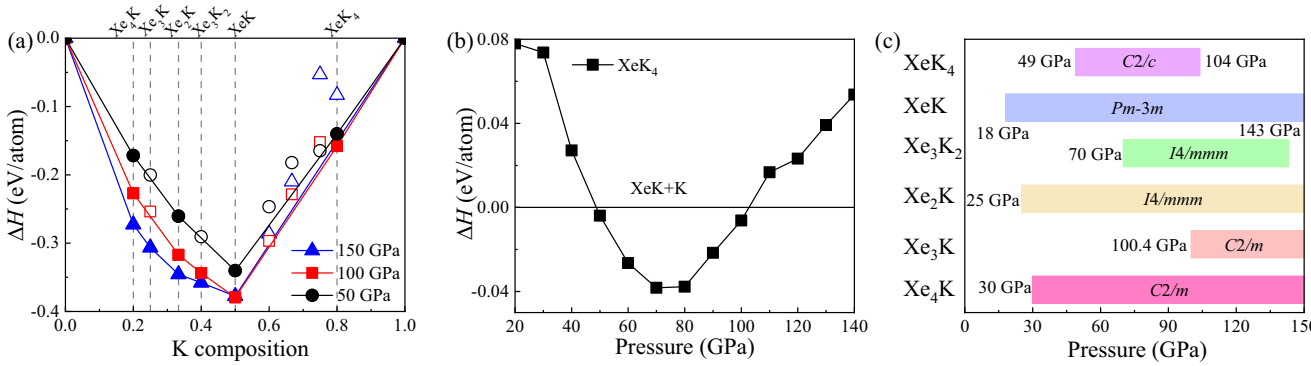

FIG. 1. (a) Convex hull of Xe_xK_y compounds at 50, 100, and 150 GPa. Solid circles, squares, and triangles represent the stable structures, while the open ones represent the unstable structures. (b) The enthalpy differences of XeK_4 with respect to Xe and XeK as a function of pressure. (c) Stable pressure ranges of predicted Xe-K compounds.

simulations reveal that $C2/c$-XeK_4 will transform into a liquid phase while other Xe-K compounds maintain their solid properties at the extreme conditions of the upper mantle of the Earth, suggesting that they might be possible constituents inside the Earth. These findings provide crucial insights into Xe chemistry as well as the interior models of the Earth.

II. COMPUTATIONAL DETAILS

The structure predictions for the Xe-K system were performed by using the particle swarm optimization algorithm as implemented in the CALYPSO code [31–34]. The CALYPSO is based on a global minimization of free-energy surfaces, designed for searching stable structures unbiased by any known structural information, and has successfully been used on various known systems, ranging from elementary to binary and ternary compounds [35–40]. The total energies of the structures were calculated in the framework of density functional theory as implemented in the VASP code [41,42], adopting the Perdew-Burke-Ernzerhof [43] parametrization under the generalized gradient approximation. Projector augmented-wave pseudopotentials with $5s^25p^6$ and $3s^23p^64s^1$ valence configurations were chosen for Xe and K atoms, respectively. The plane-wave kinetic energy cutoff was set to 600 eV and Monkhorst-Pack k-point meshes with a reciprocal space resolution of $2\pi \times 0.02$ Å^{-1} to ensure an excellent convergence of total energies and forces better than 1 meV/atom and 1 meV/Å, respectively. The phonon calculations were performed with the PHONOPY code using a finite-displacement approach [44,45]. AIMD calculations were performed in the canonical (NVT) ensemble applying a Nosé-Hoover thermostat [46] combined with a supercell method (216 atoms for Xe_2K, 250 atoms for Xe_3K_2, 250 atoms for XeK, and 240 atoms for XeK_4) with only the Γ point for the Brillouin zone sampling to determine the dynamic properties at high temperatures. Each simulation consists of 10 000 time steps with a time step of 1 fs. The crystal structures were plotted using VESTA software [47].

III. RESULTS AND DISCUSSION

We perform the systematical crystal structure searches on the stoichiometries of Xe_xK_y ($x/y = 0.25, 1/3, 0.5, 0.6, 2/3, 1, 1.5$) at pressures of 50, 100, and 150 GPa with maximum searching cells up to 4 formula units (f.u.) for each selected composition. Then we calculate about ten lowest different potential structures from all of the valid candidates which is at least 2000 for each strategy to find the potential stable stoichiometries of Xe_xK_y. Figure 1(a) shows the formation enthalpy convex hulls of all considered compositions with respect to the decomposition into Xe and K. We can clearly observe, at 50 GPa, that for the Xe-rich region, the formation enthalpies of Xe_4K, Xe_2K, and XeK lie on the convex hull, indicating the thermodynamic stability of these compounds at this pressure. As pressure increases, Xe_3K_2 and Xe_3K successively appear on the convex hull at 100 and 150 GPa, respectively, indicating that pressure induces the stability of these two compounds. This is consistent with the previously proposed theoretical Xe-K compounds under high pressure [13]. In addition to the above results, we discover an interesting stoichiometry in the K-rich region, XeK_4. Its formation enthalpy appears on the convex hull at 50 and 100 GPa, but not at 150 GPa, suggesting that the thermodynamic stability range of this stoichiometry lies within this pressure range. We calculate the relative enthalpies of XeK_4 with respect to pure XeK and Xe as a function of pressure, as shown in Fig. 1(b), and find that the predicted XeK_4 is stable in a larger range of pressure from 49 to 104 GPa. In addition, we also predict a high-pressure phase of Xe_3K, and the relative enthalpies show that this structure becomes stable when pressure is above 100.4 GPa, as shown in Fig. S1 in the Supplemental Material (SM) [48].

XeK_4 exhibits a layered crystal structure, wherein K atoms arrange in an alternating pattern, forming two layers of K atoms, while Xe atoms reside between these two K atom layers. The structure adopts a $C2/c$ crystal symmetry, as illustrated in Fig. 2. The shortest distance between K-K atoms in XeK_4 at 50 GPa is 2.55 Å, while the minimum distances between Xe-K and Xe-Xe atoms are 2.84 and 4.46 Å, respectively, at the same pressure. The phonon dispersion relation of XeK_4 at 50 GPa demonstrates the absence of imaginary frequencies across the entire Brillouin zone, indicating its dynamical stability. Electronic band structures and density of states reveal the metallic property of XeK_4, with the Fermi level predominantly occupied by electrons from K atoms. We calculated the Bader electron transition (Table S1 in the SM),

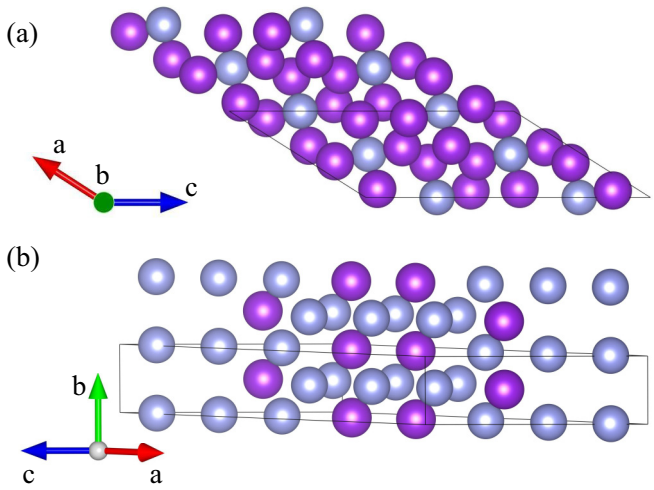

FIG. 2. The crystal structures of the two Xe-K compounds: (a) The $C2/c$ phase of XeK_4 at 50 GPa and (b) the $C2/m$ phase of Xe_3K at 100.4 GPa. The blue and purple spheres represent the Xe and K atoms, respectively.

electron localization function (ELF) (Fig. S2 in the SM), and Laplacian charge density of the predicted Xe-K compounds at selected pressures (Table S2 in the SM) to determine the electronic properties of the Xe-K compounds. We found that all Xe-K compounds exhibit typical ionic properties. For instance, each K atom in XeK_4 at 50 GPa loses 0.19 electrons, while the Xe atom gains a total of 0.76 electrons. The Laplacian charge density between Xe and K ranges from 2.18 to 2.83, indicating strong ionic bonds in Xe-K. The ELF also confirms these findings by its relatively localized electronic band structure in the Fig. 3. These results are consistent with the ionic properties observed in Xe-Na compounds under high pressure [26,27]. However, in the Na-rich system of the Na_9Xe compound, localized electrons are observed in the lattice interstices, indicating electride properties due to Xe's inability to fully accept the electrons lost from Na [27]. Given

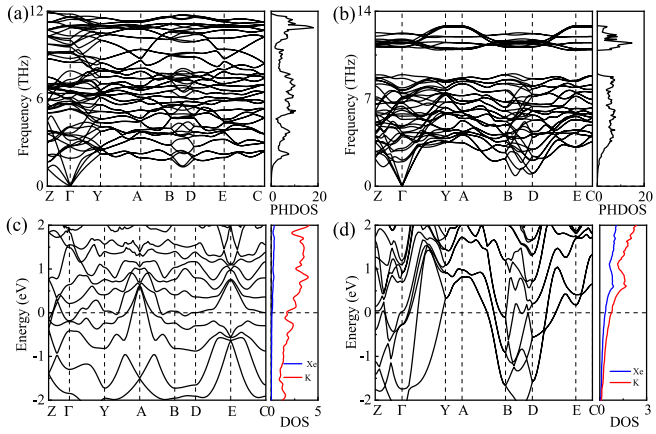

FIG. 3. Phonon dispersion relations and phonon density of states (PHDOS) for (a) XeK_4 ($C2/c$) at 50 GPa and (b) Xe_3K ($C2/m$) at 100.4 GPa. Band structures and projected density of states (DOS) of (c) XeK_4 ($C2/c$) at 50 GPa and (d) Xe_3K ($C2/m$) at 100.4 GPa. The dashed lines represent the Fermi levels.

the similarities between Xe-Na and Xe-K alloys, we predict that K-rich systems may also exhibit electride properties. We also examine possible synthesis pathways for XeK_4 under the extreme conditions. We found that K_4Fe [30] and XeO [22] are stable at high pressure within the extreme condition of the Earth's interior, and when mixed together at high pressure, they can react to form the energetically more stable XeK_4.

Previous theoretical studies suggested that Xe_3K exhibits $P4/mmm$ symmetry under pressures exceeding 100 GPa [13], whereas our predictions indicate that $C2/m$-Xe_3K is energetically more stable, as depicted in Fig. S3 in the SM. Enthalpy differences as a function of pressure show that Xe_3K stabilizes when pressure is above 100.4 GPa, with its crystal structure also displaying layered characteristics. Electronic properties confirm Xe_3K as a metal. At 100.4 GPa, each K atom in Xe_3K loses 0.12 electrons, while each Xe atom gains 0.37 electrons, elucidating the ionic bonding features of Xe-K. The detailed structural information of $C2/c$-XeK_4 and $C2/m$-Xe_3K is summarized in Table S3 in the SM. The structural configurations, phonon dispersions, and electronic properties of XeK, Xe_3K_2, and Xe_2K are also summarized in Figs. S4 and S5 in the SM. The stabilities of all the predicted Xe-K compounds are summarized in Fig. 1(c). The stable pressure range of XeK_4 (49–104 GPa) coincides precisely with that of the Earth's mantle (0–135 GPa), so then we conduct systematic AIMD to elucidate its atomic dynamical behavior at different pressures and temperatures. The mean-squared displacement (MSD) and atomic trajectories of XeK_4 are summarized in Figs. 4 and S6. It is obvious that the XeK_4 exhibits a solid character at relatively lower temperatures, as all of the Xe and K atoms in the XeK_4 vibrate at their equilibrium positions at temperature of below 2000 K under 64.0 GPa, causing their diffusion coefficient to equal zero, as shown in Fig. 4(a). As the temperature increases up to 2000 K, the ionic bonds are broken and the entire crystalline lattice melts and XeK_4 becomes a liquid, as evidenced by a linearly increasing MSD [Fig. 4(b)], indicating the transition of XeK_4 from a solid to a liquid phase. It should be noted that the heat-until-it-melts (HUM) approach [50] often overestimates the melting temperature of materials. Similar phenomena are observed under different pressures of 95.9 and 127.6 GPa, as illustrated in Fig. S6. This can also be confirmed by the calculated the radial distribution functions (RDFs) of Xe-K in XeK_4 at different pressures and temperatures, as shown in Fig. S7 in the SM. We also calculated the Gibbs free energy for all Xe-K compounds within the stable pressure and temperature ranges of XeK_4 using the quasiharmonic approximation. Combining the AIMD results, we determined the phase diagram of XeK_4, as shown in Fig. 4(c). The red circles in the phase diagram represent solid XeK_4, while the blue squares represent molten XeK_4, and the orange region represents the Earth's geotherm [49]. Through the phase diagram of XeK_4, we determined that solid XeK_4 can remain stable over a relatively large temperature and pressure range [light pink area in Fig. 4(c)]. In contrast, in the blue areas on either side of the phase diagram, the Gibbs free-energy calculations show that solid XeK_4 is not stable and will decompose into other Xe-K compounds. We roughly estimated the melting curve of XeK_4 under high temperature and high pressure, which is shown as a black dashed line in the phase diagram, although it might be overestimated. XeK_4

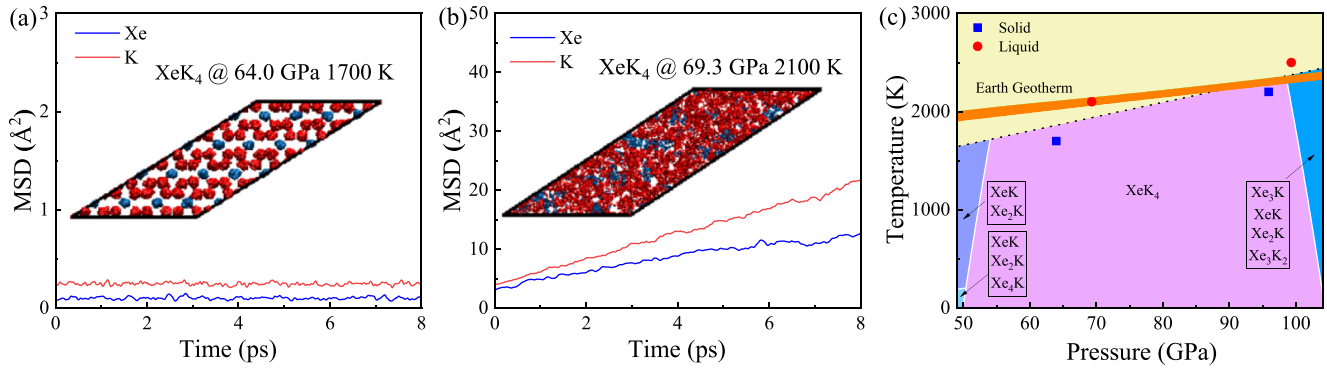

FIG. 4. The calculated mean-squared displacement (MSD) and inserted atomic trajectories for XeK_4 ($C2/c$) (a) at a pressure of 64.0 GPa and a temperature of 1700 K, and (b) at a pressure of 69.3 GPa and a temperature of 2100 K. (c) The phase diagram of XeK_4 under the extreme conditions similar to those of the inner Earth. The red circles represent solid XeK_4, while the blue squares represent molten XeK_4. The black dashed line represents the melting curve of XeK_4 and the orange region represents the Earth's geotherm [49].

will transform into a liquid phase at high temperatures, which are highlighted in yellow in the phase diagram. The HUM simulations of other materials, such as Na [50], Na-Xe [26], and SiO_2He [5], suggest that their melting temperatures are much higher than that of XeK_4, but they would eventually melt at sufficiently high temperatures.

We also examine the atomic dynamical behavior of XeK, Xe_3K_2, and Xe_2K at different pressures and temperatures, as shown in Fig. S8 in the SM. At lower temperatures, XeK, Xe_3K_2, and Xe_2K exhibit similar atomic dynamical behavior to XeK_4, with all Xe and K atoms vibrating near their lattice positions, revealing a solid phase. However, at higher temperatures (up to 4000 K), AIMD simulations reveal distinct behavior compared to XeK_4: These compounds do not transition to a liquid phase but rather remain as a solid. This phenomenon primarily arises from the presence of a greater number of Xe atoms in their crystal structures, wherein the larger atomic mass and the interactions between Xe and K hinder diffusion.

IV. CONCLUSIONS

In conclusion, we propose six unconventional Xe-K compounds under high pressure, namely Xe_4K, Xe_3K, Xe_3K_2, Xe_2K, XeK, and XeK_4. In addition to previously proposed Xe-rich compounds, a unconventional K-rich compound, XeK_4, is stable over a wide pressure range from 49 to 104 GPa and a high-pressure phase of Xe_3K. XeK_4 demonstrates metallic properties with a strong ionic Xe-K bond, and both XeK_4 and Xe_3K are dynamically stable within their stable pressure ranges. Further AIMD simulations indicate that XeK_4 undergoes a solid-to-liquid transition with increasing temperature, while the other Xe-K compounds remain solid. The solid-state stability pressure ranges of all Xe-K compounds encompass the geotherm of the Earth's mantle, implying that XeK_4 and other Xe-K compounds could potentially serve as constituents in the solid phase and exist within the Earth's mantle. These results could not only provide essential information for understanding the Earth's interior but also make contributions to the Xe chemistry.

ACKNOWLEDGMENTS

The authors acknowledge funding from the NSFC under Grants No. 12074154, No. 12174160, No. 11804128, and No. 11804129. Y.L. acknowledges the funding from the Six Talent Peaks Project and 333 High-level Talents Project of Jiangsu Province. J.H. acknowledges the funding from the Science and Technology Project of Xuzhou under Grant No. KC19010. All the calculations were performed at the High Performance Computing Center of the School of Physics and Electronic Engineering of Jiangsu Normal University.

C.L. and K.Y. contributed equally to this work.

[1] L. Zhang, Y. Wang, J. Lv, and Y. Ma, Materials discovery at high pressures, Nat. Rev. Mater. **2**, 17005 (2017).

[2] M. Xu, Y. Li, and Y. Ma, Materials by design at high pressures, Chem. Sci. **13**, 329 (2022).

[3] P. Zhang, J. Shi, W. Cui, C. Liu, S. Ding, K. Yang, J. Hao, and Y. Li, Formation of NH_3-Xe compound at the extreme condition of planetary interiors, Phys. Rev. B **105**, 214109 (2022).

[4] Y. Li, X. Feng, H. Liu, J. Hao, S. A. T. Redfern, W. Lei, D. Liu, and Y. Ma, Route to high-energy density polymeric nitrogen *t*-N via He–N compounds, Nat. Commun. **9**, 722 (2018).

[5] S. Ding, P. Zhang, K. Yang, C. Liu, J. Hao, W. Cui, J. Shi, and Y. Li, Formation of solid SiO_2-He compound at high pressure and high temperature, Phys. Rev. B **106**, 024102 (2022).

[6] J. Shi, W. Cui, J. Hao, M. Xu, X. Wang, and Y. Li, Formation of ammonia–helium compounds at high pressure, Nat. Commun. **11**, 3164 (2020).

[7] X. Dong, A. R. Oganov, A. F. Goncharov, E. Stavrou, S. Lobanov, G. Saleh, G.-R. Qian, Q. Zhu, C. Gatti, V. L. Deringer *et al.*, A stable compound of helium and sodium at high pressure, Nat. Chem. **9**, 440 (2017).

[8] F. Peng, X. Song, C. Liu, Q. Li, M. Miao, C. Chen, and Y. Ma, Xenon iron oxides predicted as potential Xe hosts in Earth's lower mantle, Nat. Commun. **11**, 5227 (2020).

[9] C. Sanloup, S. A. Bonev, M. Hochlaf, and H. E. Maynard-Casely, Reactivity of xenon with ice at planetary conditions, Phys. Rev. Lett. **110**, 265501 (2013).

[10] F. Peng, Y. Wang, H. Wang, Y. Zhang, and Y. Ma, Stable xenon nitride at high pressures, Phys. Rev. B **92**, 094104 (2015).
[11] M.-s. Miao, X.-L. Wang, J. Brgoch, F. Spera, M. G. Jackson, G. Kresse, and H.-Q. Lin, Anionic chemistry of noble gases: formation of Mg–NG (NG = Xe, Kr, Ar) compounds under pressure, J. Am. Chem. Soc. **137**, 14122 (2015).
[12] Z. Liu, J. Botana, M. Miao, and D. Yan, Unexpected Xe anions in $XeLi_n$ intermetallic compounds, Europhys. Lett. **117**, 26002 (2017).
[13] Y. Tian, S. T. John, G. Liu, and H. Liu, Predicted crystal structures of xenon and alkali metals under high pressures, Phys. Chem. Chem. Phys. **24**, 18119 (2022).
[14] S. Zhang, H. Bi, S. Wei, J. Wang, Q. Li, and Y. Ma, Crystal structures and electronic properties of cesium xenides at high pressures, J. Phys. Chem. C **119**, 24996 (2015).
[15] X. Z. Yan, Y. M. Chen, and H. Y. Geng, Prediction of the reactivity of argon with xenon under high pressures, ACS Omega **4**, 13640 (2019).
[16] M. Wang, M. A. Kuzovnikov, J. Binns, X. Li, M. Peña-Alvarez, A. Hermann, E. Gregoryanz, and R. T. Howie, Synthesis and characterization of $XeAr_2$ under high pressure, J. Chem. Phys. **159**, 134508 (2023).
[17] N. Bartlett, Xenon hexafluoroplatinate (V) $Xe^+[PtF_6]$-, Proc. Chem. Soc. **6**, 218 (1962).
[18] G. Weck, A. Dewaele, and P. Loubeyre, Oxygen/noble gas binary phase diagrams at 296 K and high pressures, Phys. Rev. B **82**, 014112 (2010).
[19] A. Dewaele, P. Loubeyre, P. Dumas, and M. Mezouar, Oxygen impurities reduce the metallization pressure of xenon, Phys. Rev. B **86**, 014103 (2012).
[20] A. Dewaele, N. Worth, C. J. Pickard, R. J. Needs, S. Pascarelli, O. Mathon, M. Mezouar, and T. Irifune, Synthesis and stability of xenon oxides Xe_2O_5 and Xe_3O_2 under pressure, Nat. Chem. **8**, 784 (2016).
[21] C. Sanloup, H.-k. Mao, and R. J. Hemley, High-pressure transformations in xenon hydrates, Proc. Natl. Acad. Sci. USA **99**, 25 (2002).
[22] Q. Zhu, D. Y. Jung, A. R. Oganov, C. W. Glass, C. Gatti, and A. O. Lyakhov, Stability of xenon oxides at high pressures, Nat. Chem. **5**, 61 (2013).
[23] A. Hermann and P. Schwerdtfeger, Xenon suboxides stable under pressure, J. Phys. Chem. Lett. **5**, 4336 (2014).
[24] M. Somayazulu, P. Dera, A. F. Goncharov, S. A. Gramsch, P. Liermann, W. Yang, Z. Liu, H.-k. Mao, and R. J. Hemley, Pressure-induced bonding and compound formation in xenon–hydrogen solids, Nat. Chem. **2**, 50 (2010).
[25] L. Zhu, H. Liu, C. J. Pickard, G. Zou, and Y. Ma, Reactions of xenon with iron and nickel are predicted in the Earth's inner core, Nat. Chem. **6**, 644 (2014).
[26] M. Zou, K. Yang, P. Zhang, W. Cui, J. Hao, J. Shi, and Y. Li, Existence of solid Na-Xe compounds at the extreme conditions of Earth's interior, Phys. Rev. Res. **5**, 043107 (2023).
[27] J. Peng, S. Wang, H. Dong, M. Wen, X. Zhang, and F. Wu, Stability of xenon-sodium compounds at moderately low pressures, Phys. Rev. B **109**, L140103 (2024).
[28] C. Sanloup, R. J. Hemley, and H. K. Mao, Evidence for xenon silicates at high pressure and temperature, Geophys. Res. Lett. **29**, 1883 (2002).
[29] W. McDonough, S.-S. Sun, A. Ringwood, E. Jagoutz, and A. Hofmann, Potassium, rubidium, and cesium in the Earth and Moon and the evolution of the mantle of the Earth, Geochim. Cosmochim. Acta **56**, 1001 (1992).
[30] A. A. Adeleke and Y. Yao, Formation of stable compounds of potassium and iron under pressure, J. Phys. Chem. A **124**, 4752 (2020).
[31] B. Gao, P. Gao, S. Lu, J. Lv, Y. Wang, and Y. Ma, Interface structure prediction via CALYPSO method, Sci. Bull. **64**, 301 (2019).
[32] Y. Wang, J. Lv, L. Zhu, and Y. Ma, CALYPSO: A method for crystal structure prediction, Comput. Phys. Commun. **183**, 2063 (2012).
[33] Y. Wang, J. Lv, L. Zhu, and Y. Ma, Crystal structure prediction via particle-swarm optimization, Phys. Rev. B **82**, 094116 (2010).
[34] X. Shao, J. Lv, P. Liu, S. Shao, P. Gao, H. Liu, Y. Wang, and Y. Ma, A symmetry-orientated divide-and-conquer method for crystal structure prediction, J. Chem. Phys. **156**, 014105 (2022).
[35] Y. Li, Y. Wang, C. J. Pickard, R. J. Needs, Y. Wang, and Y. Ma, Metallic icosahedron phase of sodium at terapascal pressures, Phys. Rev. Lett. **114**, 125501 (2015).
[36] K. Gao, W. Cui, J. Chen, Q. Wang, J. Hao, J. Shi, C. Liu, S. Botti, M. A. L. Marques, and Y. Li, Superconducting hydrogen tubes in hafnium hydrides at high pressure, Phys. Rev. B **104**, 214511 (2021).
[37] Q. Wang, W. Cui, K. Gao, J. Chen, T. Gu, M. Liu, J. Hao, J. Shi, and Y. Li, Pressure-stabilized superconducting electride Li_5C, Phys. Rev. B **106**, 054519 (2022).
[38] M. Xu, C. Huang, Y. Li, S. Liu, X. Zhong, P. Jena, E. Kan, and Y. Wang, Electrical control of magnetic phase transition in a type-I multiferroic double-metal trihalide monolayer, Phys. Rev. Lett. **124**, 067602 (2020).
[39] W. Cui, T. Bi, J. Shi, Y. Li, H. Liu, E. Zurek, and R. J. Hemley, Route to high-T_c superconductivity via CH_4-intercalated H_3S hydride perovskites, Phys. Rev. B **101**, 134504 (2020).
[40] J. Shi, W. Cui, S. Botti, and M. A. L. Marques, Nitrogen-hydrogen-oxygen ternary phase diagram: New phases at high pressure from structural prediction, Phys. Rev. Mater. **2**, 023604 (2018).
[41] G. Kresse and J. Furthmüller, Efficient iterative schemes for *ab initio* total-energy calculations using a plane-wave basis set, Phys. Rev. B **54**, 11169 (1996).
[42] A. Vanderlei dos Santos, G. Padilha, and M. Monçalves, Determination of the stability and magnetic properties of Fe–Pd nitride using the generalised gradient approximation (GGA), Solid State Sci. **14**, 269 (2012).
[43] P. E. Blöchl, O. Jepsen, and O. K. Andersen, Improved tetrahedron method for Brillouin-zone integrations, Phys. Rev. B **49**, 16223 (1994).
[44] K. Parlinski, Z. Q. Li, and Y. Kawazoe, First-principles determination of the soft mode in cubic ZrO_2, Phys. Rev. Lett. **78**, 4063 (1997).
[45] A. Togo, F. Oba, and I. Tanaka, First-principles calculations of the ferroelastic transition between rutile-type and $CaCl_2$-type SiO_2 at high pressures, Phys. Rev. B **78**, 134106 (2008).
[46] W. G. Hoover, Canonical dynamics: Equilibrium phase-space distributions, Phys. Rev. A **31**, 1695 (1985).
[47] K. Momma and F. Izumi, VESTA3 for three-dimensional visualization of crystal, volumetric and morphology data, J. Appl. Crystallogr. **44**, 1272 (2011).

[48] See Supplemental Material at http://link.aps.org/supplemental/10.1103/PhysRevB.110.024111 for structural parameters, mean-squared displacement (MSD), radial distribution functions (RDFs), Bader charges, phonon dispersion, and atomic trajectories.

[49] R. O. Pepin and D. Porcelli, Origin of noble gases in the terrestrial planets, Rev. Mineral. Geochem. **47**, 191 (2002).

[50] J.-Y. Raty, E. Schwegler, and S. A. Bonev, Electronic and structural transitions in dense liquid sodium, Nature (London) **449**, 448 (2007).